International Journal of Thermophysics, Vol. 7, No. 6, 1986

Stratified Media Theory Interpretation of Measurements of the Spectral Polarized Directional Emissivity of Some Oxidized Metals

J. M. Ane[1] and M. Huetz-Aubert[1]

Received December 9, 1985

The emissivities of metals are strongly affected by the growth of oxide films. For small film thicknesses, perturbations are limited to the visible range. As thicknesses increase, they spread to the infrared range. Various samples of optically polished metals (Fe, Ni, Cr) and stainless steels (ELI.T 1803 MoT and AISI 304 or 316) have been oxidized at temperatures ranging from 400 to 800°C. Their spectral polarized directional emissivities, $\varepsilon'_{\lambda\parallel}$ and $\varepsilon'_{\lambda\perp}$, have been measured with two experimental techniques. The spectral range studied extends from 0.4 to 14 μm; the measurement directions vary between 0 and 80° from the normal to the sample. After measurement, each sample was analyzed by glow-discharge optical spectroscopy (GDOS). From the results of the analysis and from the survey of bibliographical data, we characterized the structure of the oxide films, i.e., their approximate thicknesses and compositions. If the complex optical indices of the metals and oxides are known, the stratified media theory enables the computation of the emissivities $\varepsilon'_{\lambda\parallel}$ and $\varepsilon'_{\lambda\perp}$. Computed and measured values have been compared. It appears that the theory accounts well for experimental data when the thicknesses of the oxides are small as in stainless steels. But for thicker oxide films, discrepancies are ascribed to several reasons.

KEY WORDS: emissivity; oxidized metals; radiative properties; spectral directional emissivity; stratified media theory.

1. INTRODUCTION

Radiative properties of materials have to be more accurately evaluated as temperature levels of the operation of industrial systems increase and safety rules are enforced.

[1] Laboratoire d'Énergétique Macroscopique et Moléculaire, Combustion du Centre National de la Recherche Scientifique et de l'École Centrale des Arts et Manufactures, 92290 Chatenay-Malabry, France.

0195-928X/86/1100-1191$05.00/0

For opaque materials, knowledge of only a single directional spectral factor is required [1]; in fact, the equations [2, 3]

$$\varepsilon'_\lambda = \alpha'^{0}_\lambda = 1 - \rho'^{0\frown}_\lambda = 1 - \rho^{\circledcirc 0'}_\lambda \tag{1}$$

relate the energetic emissivity ε'_λ to the absorptivity α'^{0}_λ and reflectivities $\rho'^{0\frown}_\lambda$ and $\rho^{\circledcirc 0'}_\lambda$ [2, 3]. The subscript λ recalls that the factors are spectral; the $'$ symbol means that the flux, leaving or incident on the surface, is directional. The $\frown$ symbol indicates a flux coming from ($\rho^{\circledcirc 0'}_\lambda$) or reflected toward ($\rho'^{0\frown}_\lambda$) the whole hemisphere surrounding the sample (2π steradians). For measurements of the hemispherical-directional reflectivity $\rho^{\circledcirc 0'}_\lambda$, the incident flux must be isotropically distributed ($\circledcirc$); for absorptivity and reflectivity measurements, the incident fluxes must be depolarized (0).

When the two classical directions of polarization are considered, relations identical to Eq. (1) can be written [1] for "polarized" factors parallel ($\varepsilon'_{\lambda\|}, \alpha'_{\lambda\|}, \ldots$) or perpendicular ($\varepsilon'_{\lambda\perp}, \alpha'_{\lambda\perp}, \ldots$); furthermore,

$$\varepsilon'_\lambda = \frac{\varepsilon'_{\lambda\|} + \varepsilon'_{\lambda\perp}}{2}, \qquad \alpha'^{0}_\lambda = \frac{\alpha'_{\lambda\|} + \alpha'_{\lambda\perp}}{2}, \ldots \tag{2}$$

The radiative factors depend on the wavelength λ, direction Δ, and temperature T. They are also strongly influenced by the state of the material, i.e., surface state, impurities, grain sizes, oxidation. It is difficult to separate the effects of the different parameters. For example, oxidation and surface state are closely related; in fact, the growth of oxide grains on a polished surface may generate a rough surface.

In this work, we study the applicability of the stratified media theory [4] to the calculation of the emissivities of some oxidized metals and alloys. We used optically polished samples which were thermally oxidized at various temperatures. The emissivities are computed (Section 2) assuming that the interfaces between the oxide layers as well as the surface of the material are optically smooth. Thicknesses and compositions of the layers have been evaluated (Section 3) by glow-discharge optical spectroscopy (GDOS).

Two experimental arrangements are used to measure the radiative properties in the 0.4- to 14-μm range. They have been described elsewhere [5] and here we only summarize their principles.

(a) In the 0.4- to 3-μm and 200–1000 K ranges, the reflectivities $\rho^{\circledcirc 0'}_{\lambda\|}$ and $\rho^{\circledcirc 0'}_{\lambda\perp}$ are measured with an integrating sphere illuminated by a xenon lamp (0.4–1 μm) or a quartz–iodine lamp (1–3 μm).

(b) In the 3- to 14-μm and 400–1000 K ranges, the emissivities $\varepsilon'_{\lambda\parallel}$ and $\varepsilon'_{\lambda\perp}$ are measured by comparing the spectral fluxes emitted by the sample and a blackbody at the same temperature. In order to control the influence of the reflected parasitic fluxes, the sample is placed in a cooled tank.

Measurements of $\rho^{\textcircled{0}0'}_{\lambda\parallel}$, $\rho^{\textcircled{0}0'}_{\lambda\perp}$, $\varepsilon'_{\lambda\parallel}$, and $\varepsilon'_{\lambda\perp}$ are made for different wavelengths λ, directions Δ, and temperatures T. Metals (Fe, Ni, Cr) and stainless steels (AISI 304, 316, 1803 MoT) are previously oxidized at various temperatures. After the measurements, the samples are analyzed by GDOS. The experimental values of the spectral polarized directional emissivities $\varepsilon'_{\lambda\parallel\text{mes.}}$ and $\varepsilon'_{\lambda\perp\text{mes.}}$ are then compared to the calculated values $\varepsilon'_{\lambda\parallel\text{calc.}}$ and $\varepsilon'_{\lambda\perp\text{calc.}}$. Some of the results are presented in Section 4.

2. INTERPRETATION OF THE RADIATIVE PROPERTIES OF AN OXIDIZED ALLOY BY THE STRATIFIED MEDIA THEORY

We consider a stratified medium of M layers assumed to be homogeneous and isotropic. Each stratum is characterized by its thickness h_m, refractive index n_m, and extinction index κ_m (Fig. 1). If the interfaces

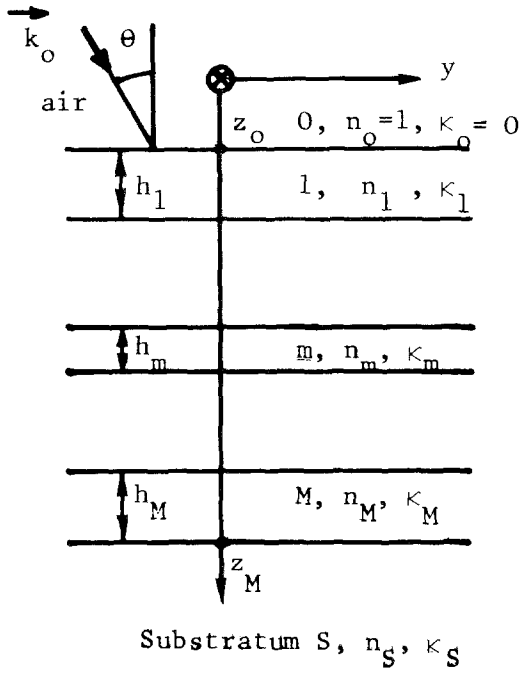

Fig. 1. Stratified medium of M layers.

are parallel and optically smooth, the reflection is specular. We assume that the substratum S is opaque. Let θ be the angle between the incident radiation and the normal to the sample.

In an absorbing layer, the wave vector $\vec{k}_m = \vec{k}'_m + i\vec{k}''_m$ is complex and its modulus is equal to

$$k_m = \frac{2\pi}{\lambda} n_m^* = \frac{\omega}{c_0}(n_m + i\kappa_m) \tag{3}$$

where c_0 is the speed of radiation in vacuum. The components of k_m in the system of axis in Fig. 1 are [3]

$$\vec{k}_m = \begin{pmatrix} 0 \\ s = k'_m \sin\theta_m = k_0 \sin\theta \\ q_m = k'_m \cos\theta_m + ik''_m \end{pmatrix} \tag{4}$$

The following can easily be shown [3].

(a) For a transverse electric (TE) wave, the components E_x of the electric field and H_y of the magnetic field satisfy the relations

$$\begin{pmatrix} E_{0x} \\ H_{0y} \end{pmatrix}_{z_0} = M^{\perp} \begin{pmatrix} E_{sx} \\ H_{sy} \end{pmatrix}_{z_M} = \begin{pmatrix} m_{11}^{\perp} m_{12}^{\perp} \\ m_{21}^{\perp} m_{22}^{\perp} \end{pmatrix} \begin{pmatrix} E_{sx} \\ H_{sy} \end{pmatrix}_{z_M} = \left(\prod_m M_m^{\perp}\right) \begin{pmatrix} E_{sx} \\ H_{sy} \end{pmatrix}_{z_M} \tag{5}$$

with

$$M_m^{\perp} = \begin{bmatrix} \cos(q_m h_m) & -i\dfrac{\omega\mu_0 \sin(q_m h_m)}{q_m} \\ -i\dfrac{q_m \sin(q_m h_m)}{\omega\mu_0} & \cos(q_m h_m) \end{bmatrix} \tag{6}$$

The magnetic permittivity μ_m of medium m is assumed to be equal to that μ_0 of vacuum.

(b) For a transverse magnetic (TM) wave, the components H_x and E_y are bound by

$$\begin{pmatrix} H_{0x} \\ E_{0y} \end{pmatrix}_{z_0} = M^{\parallel} \begin{pmatrix} H_{sx} \\ E_{sy} \end{pmatrix}_{z_M} = \begin{pmatrix} m_{11}^{\parallel} m_{12}^{\parallel} \\ m_{21}^{\parallel} m_{22}^{\parallel} \end{pmatrix} \begin{pmatrix} H_{sx} \\ E_{sy} \end{pmatrix}_{z_M} = \left(\prod_m M_m^{\parallel}\right) \begin{pmatrix} H_{sx} \\ E_{sy} \end{pmatrix}_{z_M} \tag{7}$$

with

$$M_m^{\parallel} = \begin{bmatrix} \cos(q_m h_m) & i\dfrac{\omega\varepsilon_0 n_m^{*2}\sin(q_m h_m)}{q_m} \\ i\dfrac{q_m \sin(q_m h_m)}{\omega\varepsilon_0 n_m^{*2}} & \cos(q_m h_m) \end{bmatrix} \tag{8}$$

where ε_0 is the dielectric permittivity of vacuum.

The electric field reflection factors are deduced from Eqs. (5)–(8) as follows:

$$R_\perp = \frac{[m_{11}^\perp + m_{12}^\perp(q_s/\omega\mu_0)](q_0/\omega\mu_0) - [m_{21}^\perp + m_{22}^\perp(q_s/\omega\mu_0)]}{[m_{11}^\perp + m_{12}^\perp(q_s/\omega\mu_0)](q_0/\omega\mu_0) + [m_{21}^\perp + m_{22}^\perp(q_s/\omega\mu_0)]} \tag{9}$$

$$R_\parallel = \frac{[m_{11}^\parallel - m_{12}^\parallel(q_s/\omega\varepsilon_0 n_s^{*2})](-q_0/\omega\varepsilon_0) - [m_{21}^\parallel - m_{22}^\parallel(q_s/\omega\varepsilon_0 n_s^{*2})]}{[m_{11}^\parallel - m_{12}^\parallel(q_s/\omega\varepsilon_0 n_s^{*2})](-q_0/\omega\varepsilon_0) + [m_{21}^\parallel - m_{22}^\parallel(q_s/\omega\varepsilon_0 n_s^{*2})]} \tag{10}$$

The intensity is proportional to the square of the amplitude of the electric field, and the spectral directional emissivities are given by

$$\varepsilon'_{\lambda\parallel\text{calc.}} = 1 - R_\parallel^2, \qquad \varepsilon'_{\lambda\perp\text{calc.}} = 1 - R_\perp^2 \tag{11}$$

A knowledge of the thicknesses h_m of the indices n_m and κ_m is required for the computation of $\varepsilon'_{\lambda\parallel\text{calc.}}$ and $\varepsilon'_{\lambda\perp\text{calc.}}$. The quantities n_m and κ_m can be extracted from the literature if the type of oxide formed is determined by a physicochemical analysis.

3. GLOW-DISCHARGE OPTICAL SPECTROSCOPY (GDOS). OPTICAL INDICES

In GDOS [6, 7], the sample is submitted to impacts of accelerated argon ions which extract some superficial atoms. The analysis of the resulting plasma radiation enables the determination of the sample composition. The velocity of erosion of the surface varies from 2 to 3 μm/min for the iron and stainless-steel substrates; it is closer to 1 μm/min for the oxides studied here.

Various samples were analyzed, corresponding to different metals and oxidation temperatures. We present results only for iron 400, iron 600, 304 or 316 steel 400, and 304 or 316 steel 600 samples. The 400 and 600 numbers mean that oxidation temperature is 400 and 600 Celsius degrees, respectively. The oxidation duration is 9 h.

The GDOS curves, which give the intensity of the typical radiations of

Table I. Results of GDOS on Thicknesses of Oxide Layers

Sample	Surface layer 1	Layer 2	Layer 3
Iron 400	Fe_2O_3 (0.3 μm)	Fe_3O_4 (2 μm)	
Iron 600	Fe_2O_3 (1 μm)	Fe_3O_4 (2 μm)	FeO (9 μm)
Steel 304 or 316–400	Fe_2O_3 and Cr_2O_3 (0.03 to 0.05 μm)		
Steel 304 or 316–600	Fe_2O_3 or FeO and Cr_2O_3 (0.15 to 0.25 μm)		

oxygen, chromium, and iron versus erosion duration, and literature examination (Refs. 8–10 for iron and Refs. 11 and 12 for stainless steel) lead to the results presented in Table I for the probable stratification of the samples. No significant differences have been observed between the 304 and the 316 stainless steels.

The optical indices n and κ obtained from the literature are given in Figs. 2 to 6. For Fe_2O_3, FeO, and Cr_2O_3 (Figs. 2, 3, and 4), κ tends to zero and n remains constant when λ is greater than 1 μm; these oxides may

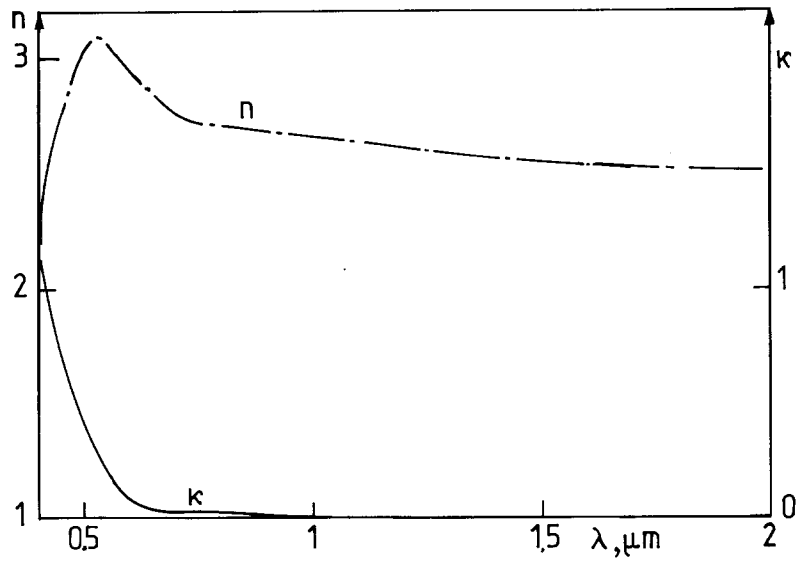

Fig. 2. Optical indices of hematite Fe_2O_3 [13]. For $\lambda > 1$ μm, $\kappa = 0$, and for $\lambda > 2$ μm, $n = 2.50$.

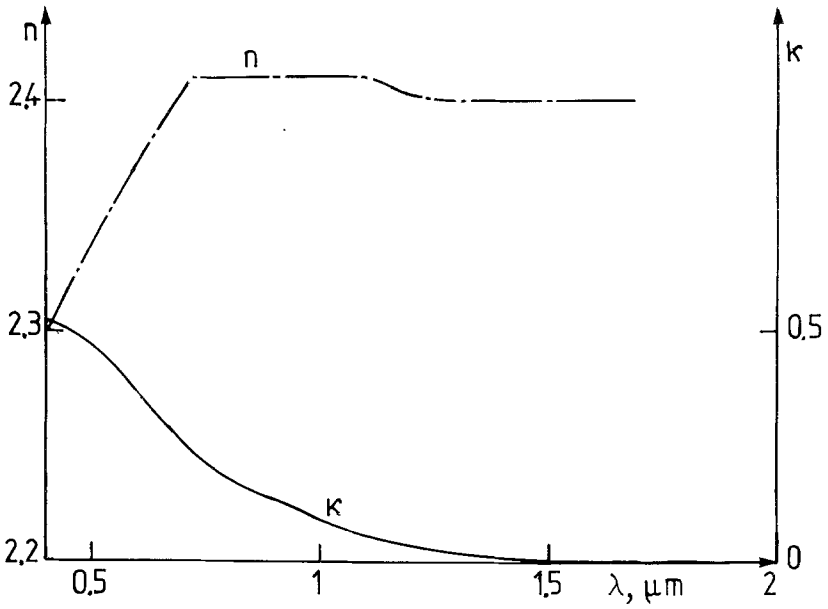

Fig. 3. Optical indices of wustite FeO [14]. For $\lambda > 1.2\ \mu m$, $n = 2.40$, and for $\lambda > 1.4\ \mu m$, $\kappa = 0$.

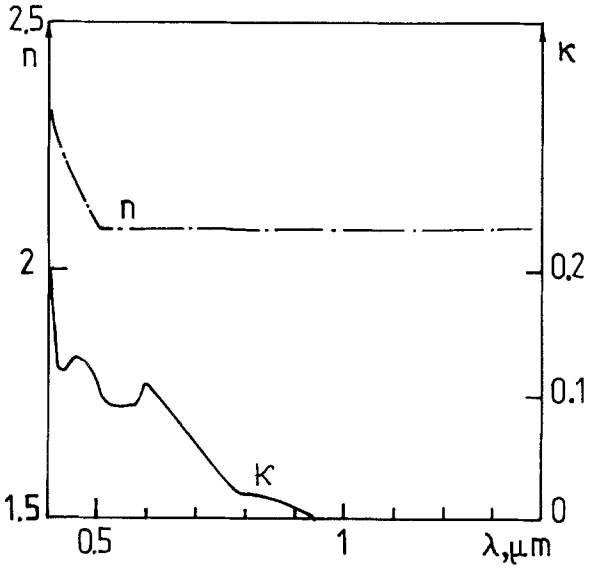

Fig. 4. Optical indices of Cr_2O_3 [13]. For $\lambda > 0.5\ \mu m$, $n = 2.08$, and for $\lambda > 0.94\ \mu m$, $\kappa = 0$.

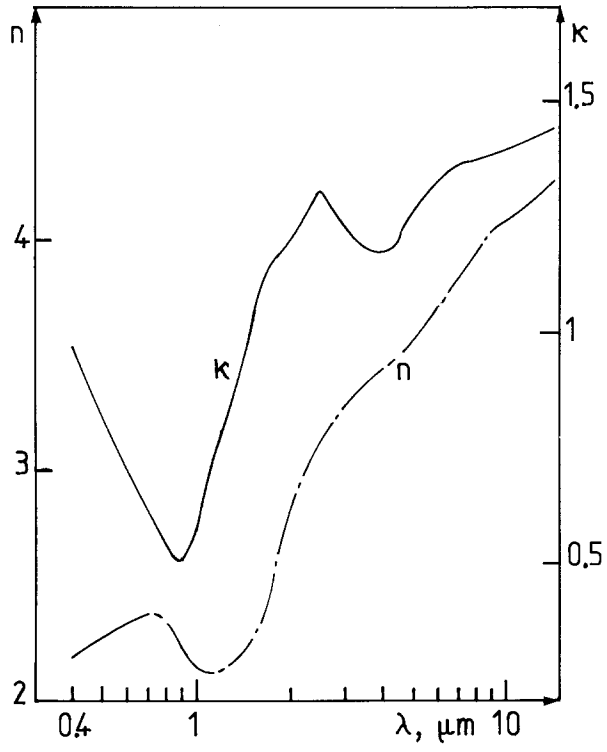

Fig. 5. Optical indices of magnetite Fe_3O_4 [15].

thus be considered as transparent in the infrared. But for Fe_3O_4 (Fig. 5) and 304 or 316 stainless steel (Fig. 6), n and κ increase with λ and a 2-μm-thick layer of Fe_3O_4 can be considered as opaque in most of the thermal spectrum. Thus the following applies.

(a) For iron 400 and iron 600 samples, the magnetite Fe_3O_4 constitutes the substrate and the radiative structure to be considered is Fe_2O_3/Fe_3O_4; the FeO layer (Table I) has no influence on the emissivity.

(b) For the stainless-steel samples, the structure to be taken into account includes two oxidized layers, the respective thicknesses of which are not evaluated by GDOS (Table I); the substrate is the stainless steel.

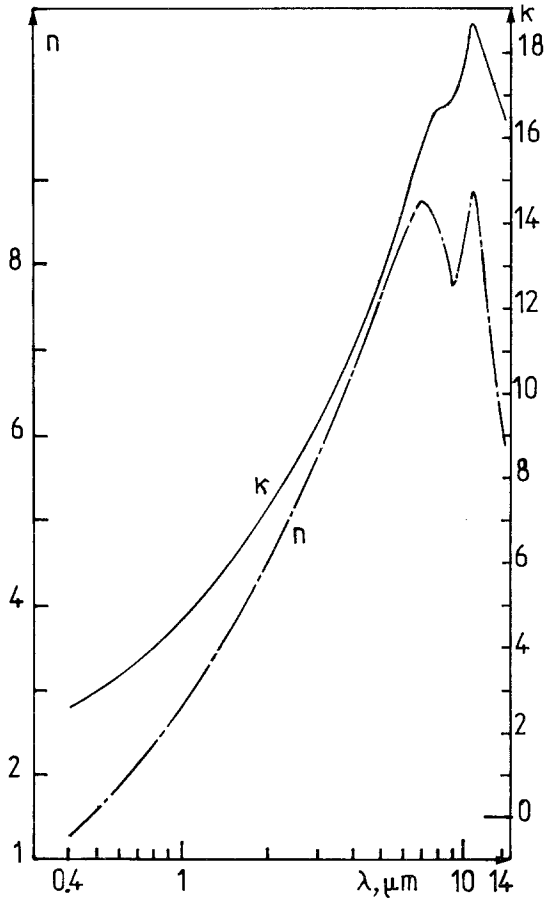

Fig. 6. Optical indices of 304 or 316 stainless steel [16].

4. COMPARISON OF THE EXPERIMENTAL AND CALCULATED EMISSIVITIES

Variations of the emissivities $\varepsilon'_{\lambda\parallel\text{mes.}}$ and $\varepsilon'_{\lambda\perp\text{mes.}}$ versus wavelength λ and direction Δ have been measured for the four samples previously presented. The measurements refer to ordinary and oxidation temperatures (400 or 600°C) whenever possible (i.e., when the integrating sphere is used) or to 400°C in the 3- to 14-μm range only. Indeed, the influence of temperature can be considered negligible, but oxidation strongly affects radiative properties.

The spectral emissivities $\varepsilon'_{\lambda\text{mes.}}(0°)$, for the direction normal to the surface of the sample ($\theta = 0°$), are presented in Figs. 7 to 10 in the 0.4- to 14-μm range. Several comments can be made.

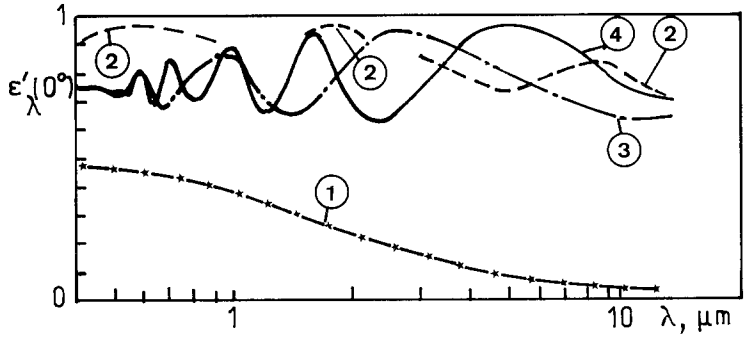

Fig. 7. Spectral emissivity of iron for the normal direction. (1) Polished unoxidized iron. (2) $\varepsilon'_{\lambda\text{mes.}}(0°)$ for iron 400. $\varepsilon'_{\lambda\text{calc.}}(0°)$ for (3) Fe_2O_3 (0.2 μm)/Fe_3O_4 and (4) Fe_2O_3 (0.4 μm)/Fe_3O_4.

(a) When the thickness of the oxide layers is less than 0.1 μm, as for the stainless steel 316–400 sample (Fig. 9), oxidation increases emissivity in the visible range but has no influence in the infrared region. So the solar flux absorbed by the steel is much greater than the flux emitted. This selectivity has been applied to the receiver of the Themis central tower solar facility [17]. $\varepsilon'_{\lambda\text{mes.}}(0°)$ varies slightly between 1.5 and 2.2 μm, depending on the temperature (curve 2a, 20°C; curves 2b and 2c, 400°C; Fig. 9). For 400°C measurements, the oxidation is probably greater although it is not evidenced by GDOS analysis.

(b) For thicker oxide layers, the stainless steel 316 sample emissivity is increased over the entire range under investigation (Fig. 10) but it still remains lower than 0.5 in the infrared. The oxide film is thicker when the

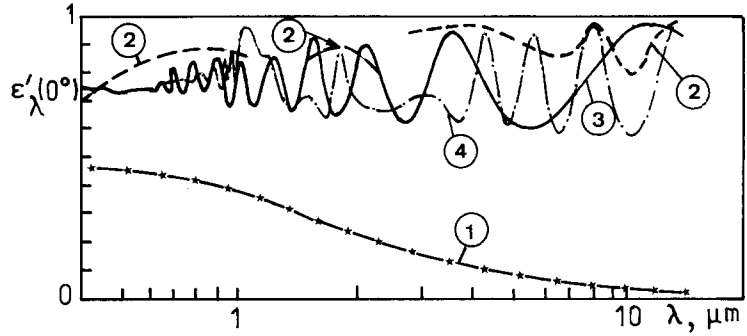

Fig. 8. Spectral emissivity of iron for the normal direction. (1) Polished unoxidized iron. (2) $\varepsilon'_{\lambda\text{mes.}}(0°)$ for iron 600. $\varepsilon'_{\lambda\text{calc.}}(0°)$ for (3) Fe_2O_3 (1 μm)/Fe_3O_4 and (4) Fe_2O_3 (4 μm)/Fe_3O_4.

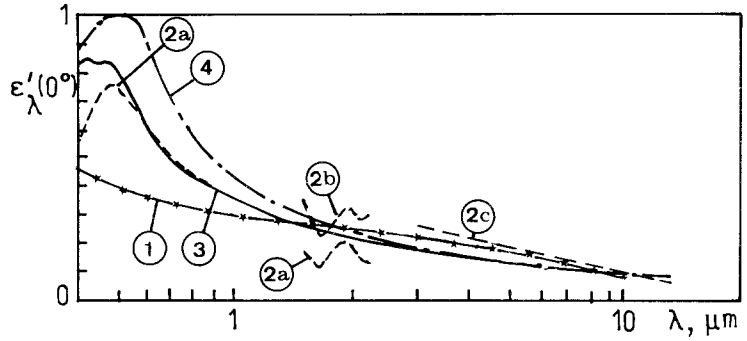

Fig. 9. Spectral emissivity of 304 or 316 stainless steel for the normal direction. (1) Polished unoxidized 304 or 316 stainless steel. $\varepsilon'_{\lambda\,\mathrm{mes.}}(0°)$ for 304 stainless steel 400; measurements at (2a) room temperature and (2b) 400°C. (2c) $\varepsilon'_{\lambda\,\mathrm{mes.}}(0°)$ for 316 stainless steel 400; measurements at 400°C. $\varepsilon'_{\lambda\,\mathrm{calc.}}(0°)$ for (3) Fe_2O_3 (0.01 μm)/Cr_2O_3 (0.005 μm)/stainless steel and (4) Fe_2O_3 (0.02 μm)/Cr_2O_3 (0.005 μm)/stainless steel.

measurements are made at 400°C (curve 2c) or 600°C (curve 2b) instead of at room temperature.

(c) For iron 400 and 600 samples (Figs. 7 and 8), the radiative properties are determined only by the oxides Fe_2O_3 and Fe_3O_4, as the Fe_3O_4 layer is opaque. Thus the emissivity is large (over 0.8) in the entire spectral range. The results show no dependence on the measurement temperature. After 9 h of oxidation, the oxide films are opaque; small variations of their thicknesses have no influence on $\varepsilon'_{\lambda\,\mathrm{mes.}}$.

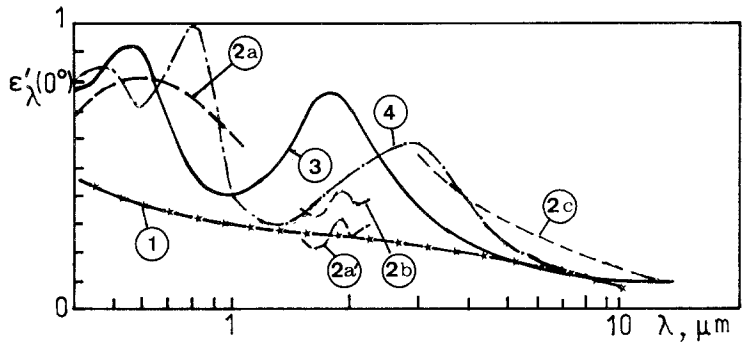

Fig. 10. Spectral emissivity of 304 or 316 stainless steel for the normal direction. (1) Polished unoxidized 304 or 316 stainless steel. (2a) $\varepsilon'_{\lambda\,\mathrm{mes.}}(0°)$ for 304 stainless steel 600; measurements at room temperature. $\varepsilon'_{\lambda\,\mathrm{mes.}}(0°)$ for 316 stainless steel 600; measurements at (2a′) room temperature, (2b) 600°C, and (2c) 400°C. $\varepsilon'_{\lambda\,\mathrm{calc.}}(0°)$ for (3) FeO (0.12 μm)/Cr_2O_3 (0.04 μm)/stainless steel and (4) FeO (0.16 μm)/Cr_2O_3 (0.08 μm)/stainless steel.

The spectral emissivities for the normal direction $\varepsilon'_{\lambda\,\mathrm{calc.}}(0°)$ have also been calculated from the stratified media theory. The optical indices were found in the literature (Figs. 2 to 6); the thicknesses and nature of the oxide were established by GDOS and comparison with published results. The GDOS accuracy in thickness determination depends on the erosion velocity, which is not well known for the analyzed samples. Consequently, thicknesses of the layers are sometimes adjusted within the possible range of values in order to adjust experimental and calculated values.

Figures 7 to 10 show that the calculated and experimental values are in general agreement. In particular, the theory accounts reasonably well for the increases in the emissivity, whether they are limited to the visible range (Figs. 9 and 10) or extend down to the infrared range (Figs. 7 and 8). For thick layers, the theory predicts interference effects which should induce rapid variations of emissivity with wavelength; we do not observe these variations (Figs. 7 and 8). In order to fit approximately experimental and calculated extrema for the iron 600 sample (Fig. 8), it is necessary to assume a thickness of 4 μm for Fe_2O_3, which is considerably above the 1 μm given by GDOS. As a general rule, it can be said that the thinner the

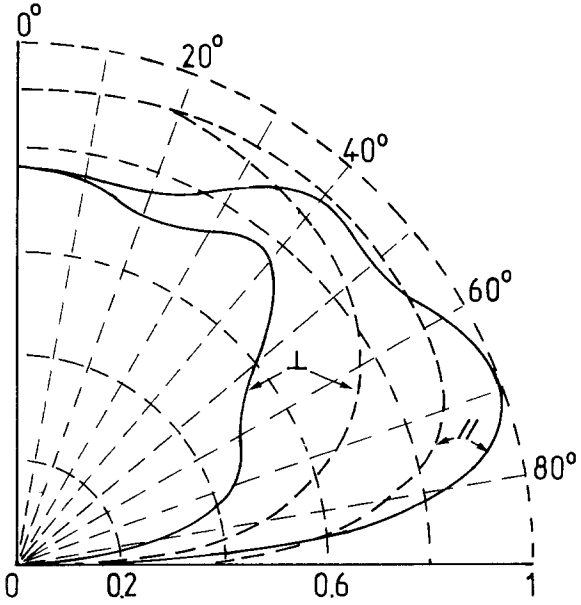

Fig. 11. Spectral directional "polarized" emissivities of iron 600 for $\lambda = 0.9$ μm. (– – –) Measured values; (——) calculated values for Fe_2O_3 (4 μm)/Fe_3O_4.

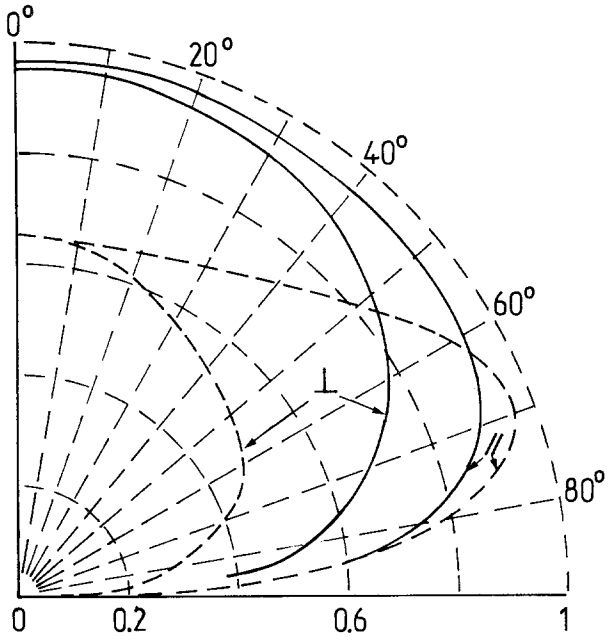

Fig. 12. Spectral directional "polarized" emissivities of iron 600 for $\lambda = 4\ \mu$m. (– – –) Calculated values for Fe_2O_3 (4 μm)/Fe_3O_4; (——) measured values.

oxide layers are, the better is the agreement between theory and measurements (Fig. 9).

The analysis of the variations of the emissivities versus the direction Δ leads to the following conclusions.

(a) The existence of a thin oxide layer does not modify the distinctive metallic aspect of curves $\varepsilon'_{\lambda\perp}(\theta)$ and $\varepsilon'_{\lambda\parallel}(\theta)$ in the infrared, with a pronounced maximum of $\varepsilon'_{\lambda\parallel}(\theta)$ close to 85° (Fig. 15). The agreement between $\varepsilon'_{\lambda\parallel\text{mes.}}$ and $\varepsilon'_{\lambda\parallel\text{calc.}}$, on the one hand, and $\varepsilon'_{\lambda\perp\text{mes.}}$ and $\varepsilon'_{\lambda\perp\text{calc.}}$, on the other hand, is quite good in the visible range (Fig. 14) and correct for λ greater than 1 μm (Fig. 15).

(b) For thicker oxide layers ($\simeq 0.20\ \mu$m), the measured values are always lower than the calculated ones for both directions of polarization (Figs. 16 and 17). However, the general aspects of experimental and theoretical curves are identical; they have the typical shape observed for a dielectric material.

(c) When the oxides turn to be opaque (for example, iron 600), the emission is almost depolarized and the $\varepsilon'_{\lambda\,\text{mes.}}(\theta)$ experimental curves are

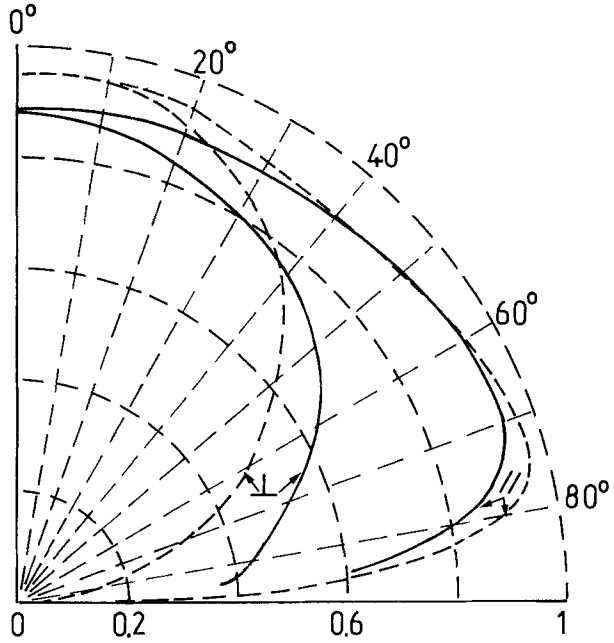

Fig. 13. Spectral directional "polarized" emissivities of iron 600 for $\lambda = 6\ \mu m$. (----) Calculated values for Fe_2O_3 (4 μm)/Fe_3O_4; (——) measured values.

closed to a circle for θ lower than 60° as can be expected (Figs. 11–13). A correct agreement between theory and experiment may casually be met, as for $\varepsilon'_{\lambda\|\text{mes.}}$ and $\varepsilon'_{\lambda\|\text{calc.}}$ at 6 μm for iron 600 (Fig. 13). But considerable differences appear for other wavelengths for the same sample (Figs. 11 and 12).

The examples presented are intended to demonstrate the usefulness of the experimental determinations of radiative properties, as a function of wavelength, direction, and state of polarization, in order to validate a model. A similar conclusion was drawn in Ref. 18.

The discrepancies observed between experimental results and theory can be ascribed to the following reasons.

(a) Even if the oxide layers are homogeneous and isotropic and if, for example, Fe_2O_3 and Fe_3O_4 oxides grow separately without reciprocal interdiffusion, the interface is probably not as smooth as was the surface of the polished unoxidized metal. The roughness of interfaces may be responsible for the nonspecularity of the reflection; it damps the interference effects and is all the more important as the oxide thickness increases, which

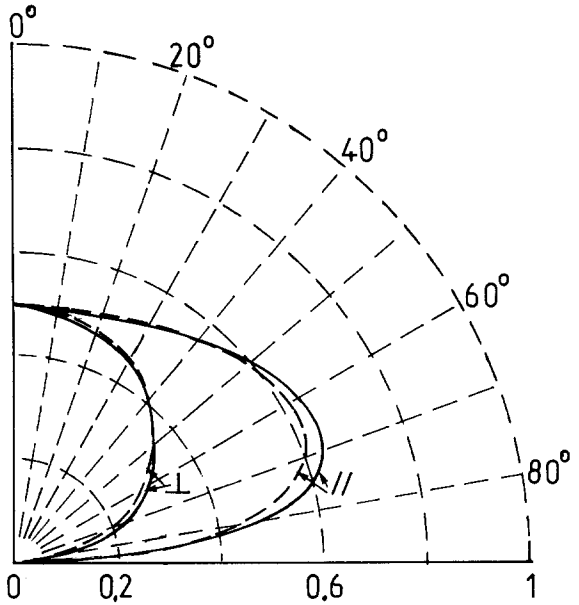

Fig. 14. Spectral directional "polarized" emissivities of 304 stainless steel 400 for $\lambda = 0.7$ μm. (– – –) Measured values; (——) calculated values for Fe_2O_3 (0.01 μm)/Cr_2O_3 (0.005 μm)/stainless steel.

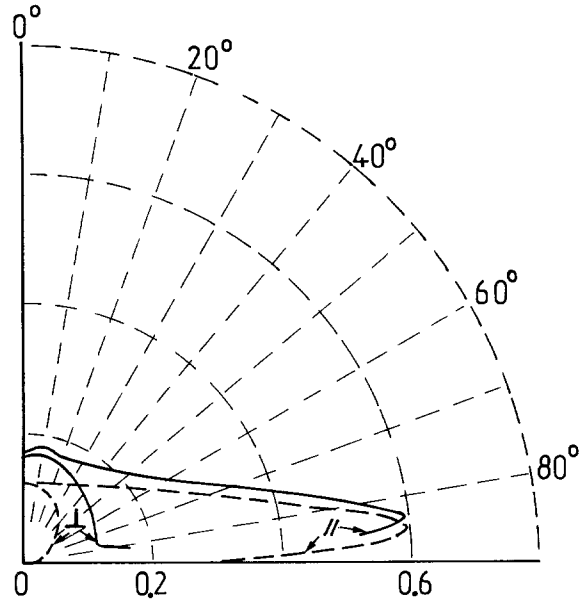

Fig. 15. Spectral directional "polarized" emissivities of 316 stainless steel 400 for $\lambda = 6$ μm. (– – –) Measured values; (——) calculated values for Fe_2O_3 (0.01 μm)/Cr_2O_3 (0.005 μm)/stainless steel.

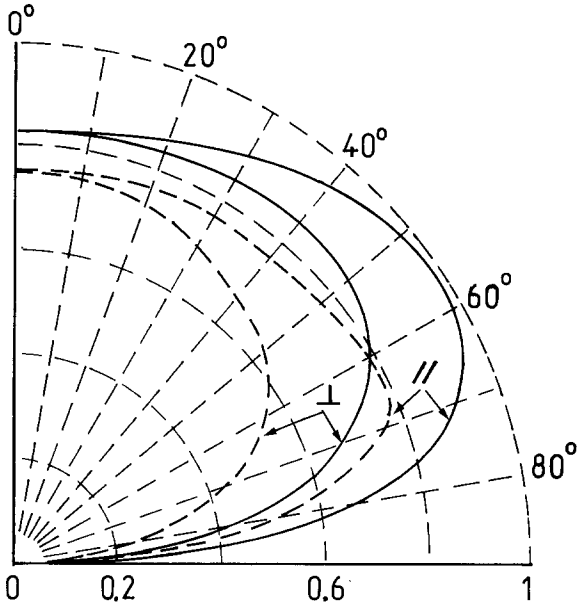

Fig. 16. Spectral directional "polarized" emissivities of 304 stainless steel 600 for $\lambda = 0.7$ μm. (----) Measured values; (——) calculated values for FeO (0.16 μm)/Cr_2O_3 (0.08 μm)/stainless steel.

explains the increase in discrepancies between theory and experiment as oxide layers grow.

(b) Literature on optical indices is scarce and the values given by the different authors vary over a wide range. All the more, the rare determinations of n and κ are usually made at ordinary temperatures and for pure materials. The measurement temperatures and the impurities diffused into the oxides during the oxidation process may strongly influence the values of the indices. In particular, it is well known that impurities tend to increase the extinction indice κ in the infrared. For most oxides (Figs. 2–4), except for Fe_3O_4 (Fig. 5), κ is low and is close to zero for λ greater than 1 μm; the measurement of low κ is difficult and may be partially responsible for the discrepancies observed.

(c) Only one surface analysis method (GDOS) was used, which is not enough to determine the exact structure of the superficial layers, in particular the values of the thicknesses and the exact composition of the strata.

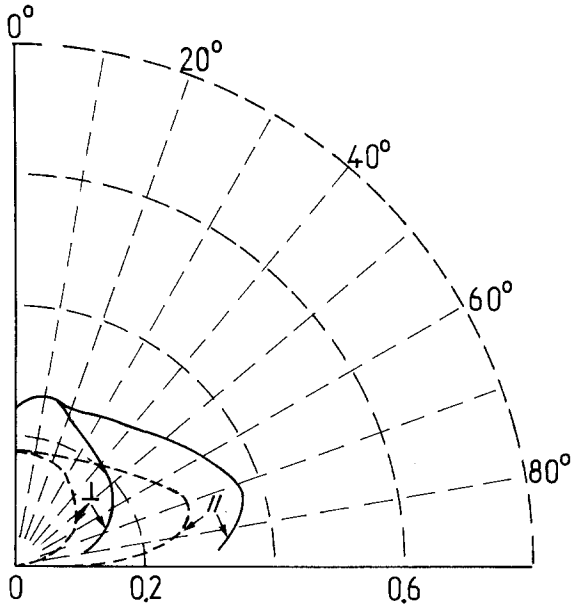

Fig. 17. Spectral directional "polarized" emissivities of 316 stainless steel 600 for $\lambda = 6\ \mu m$. (----) Measured values; (——) calculated values for FeO (0.16 μm)/Cr_2O_3 (0.08 μm)/stainless steel.

5. CONCLUSION

Due to the sensitivity of the radiative properties to the surface state, it is difficult to find reliable data in the literature. One is often faced with the problem of needing numerical values for the evaluation of radiative energy transfers. For metallic compounds, oxidation strongly influences the spectral polarized directional emissivities in the visible range but has no effect in the infrared when the oxide thicknesses are small; in this case, the stratified media theory gives a good interpretation of experimental data, as the hypotheses underlying it (i.e., homogeneous and isotropic media, parallel and smooth interfaces) are realistic. For larger oxide thicknesses, emissivities are increased over the entire spectrum and the calculated factors do not fit the experimental ones. The use of more sophisticated theories implies an improvement of the measurement of radiative properties (in particular, the proportion of light diffusely reflected has to be evaluated) and of the optical indices (which are often computed from reflectivity measurements), as well as better material characterization techniques.

REFERENCES

1. R. Siegel and J. R. Howell, *Thermal Radiation Heat Transfer* (McGraw–Hill, New York, 1981).
2. M. Huetz-Aubert and J. Taine, *Rev. Gen. Therm.* **17**:755 (1978).
3. J. M. Ané, Thèse Docteur Ingénieur (École Centrale des Arts et Manufactures, Paris, Nov. 1984).
4. F. Abélès, *Ann. Phys.* **3**:504 (1948).
5. J. M. Ané, J. F. Sacadura, and P. Stekelorom, *VIIth Int. Heat Transfer Conf.*, Munich, Germany, 1982.
6. R. Berneron and J. C. Charbonnier, *Surface Interface Anal.* **3**:135 (1981).
7. J. E. Greene and J. M. Whelan, *J. Appl. Phys.* **44**:2509 (1973).
8. D. L. Douglass and R. B. Pettit, *Sol. Energy Mat.* **4**:383 (1981).
9. B. E. F. Fender and F. D. Riley, *J. Phys. Chem. Solids* **30**:793 (1969).
10. J. Bernard, *L'Oxydation des Métaux* (Gauthier Villars, Paris, 1962).
11. G. Betz, G. K. Wehner, L. Toth, and A. Joshi, *J. Appl. Phys.* **45**:230 (1974).
12. C. Ducrocq, Thèse d'État (Orsay, June 1982).
13. B. Karlsson, C. G. Ribbing, A. Roos, E. Valkonen, and T. Karlsson, *Phys. Scr.* **25**:826 (1982).
14. A. I. Galuza, V. V. Eremenko, A. P. Kirichenko, and V. A. Konstantinov, *Sov. Phys. Solid. State* **23**:140 (1981).
15. A. Schlegel, S. F. Alvarado, and P. Watchter, *J. Phys. C* **12**:1157 (1979).
16. Tran N'Guyen Hiep, Thèse Docteur Ingénieur (École Centrale des Arts et Manufactures, Paris, June 1981).
17. P. Stekelorom, Thèse Docteur Ingénieur (École Centrale des Arts et Manufactures, Paris, Sept. 1983).
18. P. Demont, M. Huetz-Aubert, and H. Tran N'Guyen, *Int. J. Thermophys.* **3**:335 (1982).

Printed in Belgium